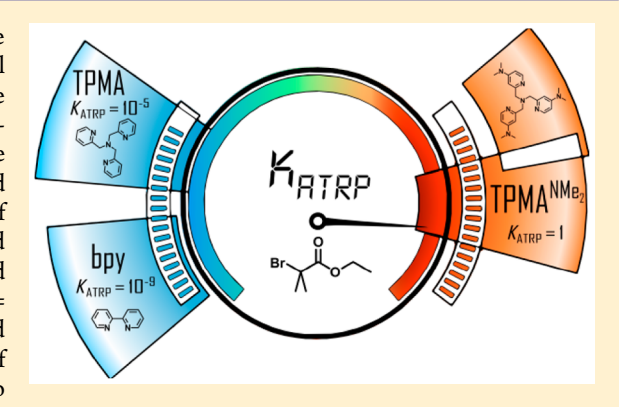


Synthesis and Characterization of the Most Active Copper ATRP Catalyst Based on Tris[(4-dimethylaminopyridyl)methyl]amine

Thomas G. Ribelli,^{†,‡} Marco Fantin,^{†,‡} Jean-Claude Daran,[§] Kyle F. Augustine,[†] Rinaldo Poli,^{§,||} and Krzysztof Matyjaszewski*,†

Supporting Information

ABSTRACT: The tris[(4-dimethylaminopyridyl)methyl]amine (TPMANMe2) as a ligand for copper-catalyzed atom transfer radical polymerization (ATRP) is reported. In solution, the [Cu^I(TPMA^{NMe2})Br] complex shows fluxionality by variable-temperature NMR, indicating rapid ligand exchange. In the solid state, the [Cu^{II}(TPMA^{NMe2})Br][Br] complex exhibits a slightly distorted trigonal bipyramidal geometry ($\tau = 0.89$). The UV-vis spectrum of [Cu^{II}(TPMA^{NMe2})Br]⁺ salts is similar to those of other pyridine-based ATRP catalysts. Electrochemical studies of [Cu(TPMA^{NMe2})]²⁺ and $[Cu(TPMA^{NMe2})Br]^+$ showed highly negative redox potentials $(E_{1/2} =$ -302 and -554 mV vs SCE, respectively), suggesting unprecedented ATRP catalytic activity. Cyclic voltammetry (CV) in the presence of methyl 2-bromopropionate (MBrP; acrylate mimic) was used to determine activation rate constant $k_a = 1.1 \times 10^6 \,\mathrm{M}^{-1} \,\mathrm{s}^{-1}$, confirming



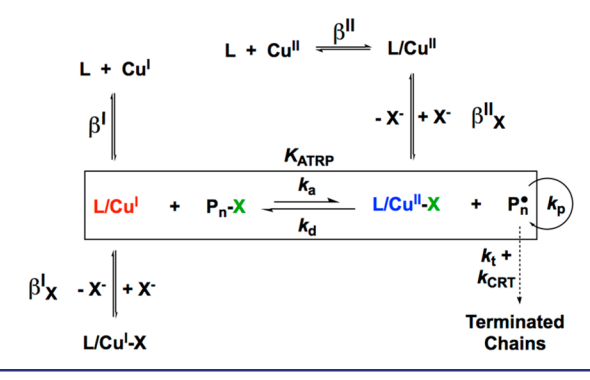
the extremely high catalyst reactivity. In the presence of the more active ethyl α -bromoisobutyrate (EBiB; methacrylate mimic), total catalysis was observed and an activation rate constant $k_a = 7.2 \times 10^6 \, \mathrm{M}^{-1} \, \mathrm{s}^{-1}$ was calculated with values of $K_{\mathrm{ATRP}} \approx 1$. ATRP of methyl acrylate showed a well-controlled polymerization using as little as 10 ppm of catalyst relative to monomer, while side reactions such as Cu^I-catalyzed radical termination (CRT) could be suppressed due to the low concentration of L/Cu^I at a steady state.

INTRODUCTION

Atom transfer radical polymerization (ATRP) has gained widespread use due to its easy setup, tolerance to functional groups, mild conditions, and wide range of applications. 1-4 Since its inception in 1995, when stoichiometric amounts of airsensitive Cu^I relative to alkyl halide initiator were used, 5 many advances have been made to improve the efficiency of this polymerization system.⁶ The development of new operating techniques such as initiators for continuous activator regeneration (ICAR) ATRP,^{7,8} activators regenerated by electron transfer (ARGET) ATRP,⁹⁻¹¹ supplemental activators and reducing agents (SARA) ATRP, 12 as well as photo-ATRP, 13-17 eATRP, 18 and most recently mechanoATRP 19,20 have allowed polymerizations to be conducted using parts per million levels of catalyst relative to monomer.

As shown in Scheme 1, the control in ATRP is achieved via a reversible redox equilibrium between a L/Cu^{I/II} couple where L signifies a multidentate nitrogen-based ligand. L/CuI activates a (macro)alkyl halide chain end, resulting in the L/Cu^{II}-X deactivator and a carbon-based radical, 21 which propagates by adding to monomer before being trapped by the L/Cu^{II}-X

Scheme 1. Mechanism of ATRP (boxed) and Equilibria Involving Association of Ligand (β^{m}) and Halide (β^{m}_{x}) to Either the Cu^{I} (m = I) or Cu^{II} (m = II) Ion



deactivator, regenerating the L/Cu^I species and the dormant polymer chain.⁴ To control the polymerization,²² this

Received: November 27, 2017 Published: January 10, 2018

Department of Chemistry, Carnegie Mellon University, 4400 Fifth Avenue, Pittsburgh, Pennsylvania 15213, United States §CNRS, LCC (Laboratoire de Chimie de Coordination), Université de Toulouse, UPS, INPT, 205 Route de Narbonne, F-31077 Toulouse Cedex 4, France

Institut Universitaire de France, 1 Rue Descartes, 75231 Paris Cedex 05, France

equilibrium $(K_{\rm ATRP})$ should lie on the dormant side to diminish the concentration of radicals and retain chain-end functionality (CEF). $K_{\rm ATRP}$ can be expressed as the ratio of activation $(k_{\rm a})$ to deactivation $(k_{\rm d})$ rate constants and can be tuned over 8 orders of magnitude²³ based on temperature, pressure, solvent,^{24,25} polymer chain end,²⁶ and choice of catalyst.²³ In order to reach even lower catalyst loadings or to polymerize less active monomers such as vinyl acetate $({\rm VAc})$,²⁷ higher values of $K_{\rm ATRP}$ must be achieved.

One simple way to tune ATRP is by changing the coordination sphere of copper. Over the years, rational ligand design has allowed for the understanding of how the catalyst structure affects reactivity. The activity of the catalyst in ATRP correlates with ligand denticity, nature of the N-donor atom, and electron-donating ability through the coordinating nitrogen atom(s).²⁸ Indeed, a linear correlation between the redox potential $(E_{1/2})$ and $ln(K_{ATRP})$ has been established where a more negative $E_{1/2}$ results in a larger value of K_{ATRP} . ²⁹ This strong correlation allows for the prediction of new catalysts' activity based solely on their redox potential. The activity of a catalyst can also be further assessed by comparing the stability constants (binding constants), β , of the L/Cu^{II} and L/Cu^{II} complexes since K_{ATRP} scales with the $\beta^{\text{II}}/\beta^{\text{I}}$ ratio, as shown in Scheme 1. While both β^{II} and β^{I} should be large, β^{II} must be $>\beta^{I}$ in order to provide a thermodynamic driving force for alkyl halide activation.²⁹ Indeed, β^{I} values are rather constant, but β^{II} values change significantly with the ligand structures.³

To date, the most active ATRP catalyst has used the ligand tris[((4-methoxy-2,5-dimethyl)-2-pyridyl)methyl]amine (TPMA*³), which has three electron-donating groups on each pyridine ring. This led to a catalyst that is 5 million times more active than the seminal catalytic system employing the 2,2′-bipyridine (bpy) ligand and 1000 times more active than the commonly used tris(pyridylmethyl)amine (TPMA) ligand (Scheme 2).

Scheme 2. Structure of the Ligands Used in This Study

According to Hammett parameters, using the even more electron-donating dimethyl amino (-NMe₂) group should further increase the catalyst activity as already observed for bpy derivatives.³³ Therefore, we considered using tris[(4-dimethylamino-2-pyridyl)methyl]amine (TPMA^{NMe2}) ligand as shown in Scheme 2.^{34–36} This ligand was previously reported by Karlin et al., where the [Cu^I(TPMA^{NMe2})]⁺ complex was used as an oxygen activation catalyst to mimic various coppercontaining enzymes^{37,38} such as amine oxdiases,³⁹ multicopper oxidases⁴⁰ (MCOs), and tyrosinases⁴¹ as well as to study this complex's interactions with carbon monoxide.⁴² This new Cubased ATRP catalyst with TPMA^{NMe2}, in both relevant oxidation states, has been characterized in solution and the solid state and utilized in ATRP systems with low catalyst loadings (down to 10 ppm) and was shown to exhibit unprecedented reactivity with alkyl halides.

RESULTS AND DISCUSSION

TPMA^{NMe2} was prepared by a procedure slightly modified from that used by Karlin et al.³⁴ (Scheme S1). The synthesis of 2-hydroxymethyl-4-dimethylaminopyridine (2; Scheme S1) was conducted as previously published by Comba et al.³⁵ The synthesis of 2-phthalimidomethyl-4-chloropyridine (5; Scheme S1) was conducted as previously published by our group.³¹ 2-Aminomethyl-4-dimethylpyridine (6; Scheme S1) was synthesized directly from a basic workup of 2-phthalimidomethyl-4-dimethylaminopyridine. It should be noted that it is very important to use a chemical-resistant O-ring (ACE glass 7855-813) for reactions using high-pressure tubes. The ligand has been characterized by ¹H/¹³C NMR and ESI-MS, which confirmed the predicted structure.

Variable-Temperature NMR of Cu^I Complexes. It has been previously shown that L/Cu^I complexes with multidentate pyridine-based ligands can undergo fast ligand exchange in the presence of excess ligand relative to $Cu^{I.43}$ The solution prepared by addition of TPMA NMe2 to CuBr was studied by variable-temperature NMR, as shown in Figure 1.

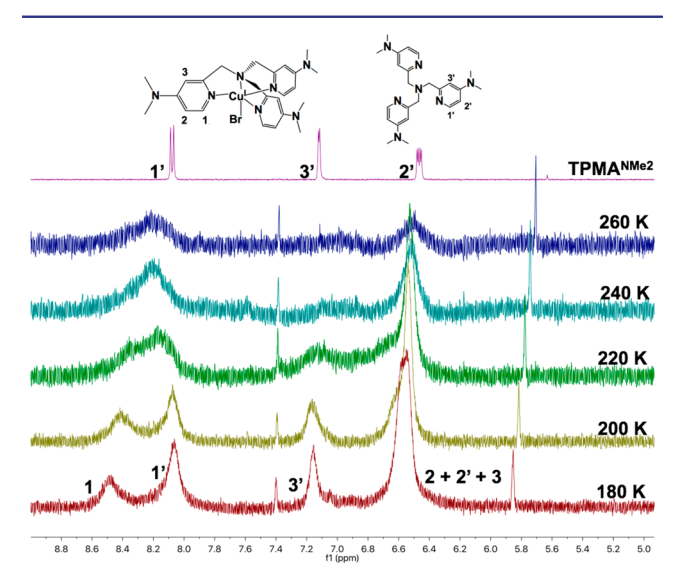


Figure 1. Variable-temperature ¹H NMR of the aromatic region of the free TPMA^{NMe2} ligand and its CuBr complex at the molar ratio $[\text{CuBr}]_0$: $[\text{TPMA}^{\text{NMe2}}]_0 = 1:3$ in d_6 -acetone.

Upon reacting equimolar amounts of TPMANMe2 and CuBr in d_6 -acetone, the reaction initially turned to a pale-yellow color, common for Cu^I complexes coordinated by pyridinic ligands. However, upon stirring, the reaction mixture turned green along with a dark precipitate indicative that the $[Cu^I(TPMA^{NMe2})Br]$ complex underwent disproportionation to [Cu^{II}(TPMA^{NMe2})Br][Br] and Cu⁰ + TPMA^{NMe2}. Typically, unsubstituted TPMA shows little to no disproportionation. The position of the disproportionation equilibrium, $K_{\text{Disp,LCw}}$ depends on the relative stability of L/Cu^{II} compared to L/ Cu^I. Since TPMA^{NMe2} stabilizes Cu^{II} much more than TPMA, disproportionation is possible. This is especially true in a disproportionating solvent such as acetone, which is polar and coordinates weakly to Cu^I. ²⁹ To suppress disproportionation and reform the [Cu^I(TPMA^{NMe2})Br] complex, 2 additional equivalents of TPMANMe2 were added. 44 Indeed, upon further stirring for 30 min, the reaction regained its yellow color and the Cu⁰ particles were no longer visible.

The ¹H NMR spectrum shows significant broadening of the aromatic peaks upon complexation, which has been previously been shown for other Cu^I complexes. 45-47 This broadening indicates a fast exchange between free and coordinated ligand. Upon decreasing the temperature to 240 K, the peaks attributed to coordinated and uncoordinated ligand began to resolve due to the slower rate of exchange. At 180 K, two distinct peaks were observed at 8.05 and 8.5 ppm, attributed to free and coordinated ligand, respectively. 43,48-51 The peaks became narrower at lower temperature but were broader than those of previously published TPMA-based Cu^I complexes at 180 K. This could be due to the presence of small amounts of paramagnetic CuII formed from disproportionation and plausible self-exchange between the CuII and the CuI complexes. This cannot be avoided due to the disproportionating nature of acetone and the highly reactive $[Cu^{I}(TPMA^{NMe2})]^{+}$ complex. Although the variable-temperature NMR spectra indicate a significant amount of ligand exchange, the total amount of uncoordinated Cu is extremely low due to the large stability constants, β^{I} , as has been previously observed for substituted TPMA ligands. 43

Structural Studies of Cull Deactivator Complex. The $[Cu^{II}(TPMA^{NMe2})Br]^+$ complex was synthesized and crystallized as reported in the Supporting Information. The resulting molecular structure is presented in Figure 2 with selected bond distances and angles summarized in Table 1.

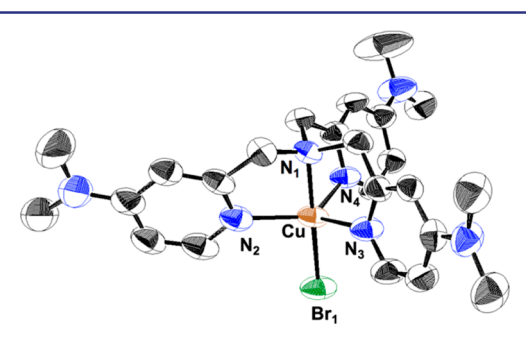


Figure 2. Molecular structure of [Cu^{II}(TPMA^{NMe2})Br][Br] shown (left) with 50% probability displacement ellipsoids. H atoms, counter Br anion, and solvent molecules have been omitted for clarity.

The [Cu^{II}(TPMA^{NMe2})Br]⁺ cation is in a slightly distorted trigonal bipyramidal geometry, indicated by a structural parameter $\tau = 0.89$ ($\tau = 1.00$ for trigonal bipyramidal). Coordination of the tetradentate ligand occurs through three substituted pyridinic nitrogen atoms in the equatorial plane (N_{eq}) and a central anchoring aliphatic nitrogen in the axial plane (Nax). The Nax-Cu-Neq bond angles are all slightly smaller than 90°, which is consistent with a previously reported cupric aqua adduct, 36 [Cu^{II}(TPMA^{NMe2})(H₂O)]²⁺. The similar N_{ax} -Cu- N_{eq} angles between the two complexes, although with differently sized axial ligands (Br vs H2O), suggest these deviations from 90° are most likely due to the natural bite of the ligand as opposed to steric repulsion from the axial ligand. The previously reported⁴² cuprous carbonyl adduct, [Cu^I(TPMA^{NMe2})(CO)]⁺, showed a Cu^I-N_{ax} bond distance of 2.446 Å, which is significantly elongated compared to the $\text{Cu}^{\text{II}}\text{--}\text{N}_{\text{ax}}$ bond distance of 2.05 Å presented in this study. Although the two complexes cannot be directly compared due to the difference in axial ligand, Cu-N_{ax} bond elongation upon reduction of Cu^{II} to Cu^I has been observed in other TPMA-based complexes.⁵² This is attributed to Cu^{II} preferring a 5coordinate environment, while the reduced Cu^I ion prefers 4coordinate geometries.⁵³ Thus, the Cu^I-N_{ax} bond is elongated to a nonbonding distance forming a distorted tetrahedral geometry. Furthermore, as shown in Figure S5, the crystal structure is stabilized by $\pi - \pi$ stacking interactions between substituted pyridine rings as well as weak C-H---Br (2.84 Å) interactions.

Solution Studies of Cu^{II} Complexes. The UV-vis-NIR spectra were obtained using CuBr₂ to form [Cu^{II}(TPMA^{NMe2})-Br]+ and also Cu(OTf)₂ to form [Cu^{II}(TPMA^{NMe2})-(MeCN)]2+, since the OTf- anion coordinates very weakly to the Cu^{II} center in solution. As shown in Figure 3A, two d \rightarrow d transitions are observed in the NIR and visible region at 1038 and 776 nm for the [Cu^{II}(TPMA^{NMe2})Br]⁺ complex and 980 and 725 nm for the [Cu^{II}(TPMA^{NMe2})(MeCN)]²⁺ complex, respectively. These two transitions are typical of d⁹ Cu^{II} possessing trigonal bipyramidal geometry and are attributed to $d_{xz} \approx d_{yz} \rightarrow d_{z2}$ and to $d_{x2-y2} \approx d_{xy} \rightarrow d_{z2}$. S4,55 A ligand to metal charge transfer (LMCT) band is apparent in both complexes, centered around 425 and 395 nm for $[Cu^{II}(TPMA^{NMe2})Br]^+$ and $[Cu^{II}(TPMA^{NMe2})(MeCN)]^{2+}$, respectively. The absorption spectra of these two complexes are consistent with previously published results for many ATRP deactivator complexes presenting trigonal bipyramidal geometry. 43,50

A sample of [Cu^{II}(TPMA^{NMe2})Br][Br] crystals was also investigated, after dissolution into a dichloromethane (DCM)/ toluene mixture, by X-band EPR spectroscopy at 120 K as shown in Figure 3B. The spectrum revealed a pattern and g/Aparameters rather close to those of the related [Cu^{II}(TPMA)-Br]+ complex.⁵⁷ On the other hand, a rather uninformative cubit tensor at g = 2.123 and a line width of ca. 110 G without observable copper hyperfine coupling was observed in pure MeCN or pure DCM as shown in Figure S4.

Thermodynamic Parameters. As noted above, one method to determine catalyst activity in ATRP is by measuring the stability constants, β^{I} and β^{II} , for the L/Cu^{II} and L/Cu^{II} complexes.⁴³ The redox potential of the $[Cu(L)]^{2+}$ complex gives the β^{II}/β^{I} ratio as shown in eq 1, where $E^{\circ}_{Cu^{2+}/Cu^{+}}$ and $E_{\text{LCu}^{\text{II}}/\text{LCu}^{\text{I}}}^{\circ}$ represent the standard redox potential of solvated Cu and the ligated Cu species, respectively.⁵⁸ Furthermore, according to eq 2, it is also possible to obtain the ratio $\beta_{X,app}^{II}/\beta_{X,app}^{I}$ electrochemically, where $\beta_{X,app}^{II}$ and $\beta_{X,app}^{I}$ are the apparent equilibrium constants of halide association to ligated copper, L/Cu^{II}–X or L/Cu^I–X, respectively. ⁴³ $\beta_{X,app}^{II}$ considers that addition of X⁻ does not change the original β^{I} and β^{II} values. For efficient deactivation, β_X^{II} values must be high. Values of β_X^I should be low, since $[Cu^I(L)Br]$ is an inefficient activator

$$\ln \frac{\beta^{\rm I}}{\beta^{\rm II}} = \frac{F}{RT} (E^{o}_{\rm Cu^{2+}/Cu^{+}} - E^{o}_{\rm LCu^{II}/LCu^{I}})$$
 (1)

$$\ln \frac{\beta_{X,app}^{II}}{\beta_{X,app}^{I}} = \frac{F}{RT} (E_{LCu^{II}/LCu^{I}}^{o} - E_{LCu^{II}-X/LCu^{I}-X}^{o})$$
(2)

As shown in Figure 4, both the $[Cu(TPMA^{NMe2})(MeCN)]^{2+}$ and the $[Cu(TPMA^{NMe2})Br]^+$ complexes exhibit a reversible redox wave at $E_{1/2} = -302$ and -554 mV vs SCE, respectively, representing the most reducing ATRP catalysts to date. Separation between the anodic and the cathodic peaks is ca. 60 mV at a scan rate of 0.2 V s⁻¹, indicating good reversibility. Increasing the scan rate results in the expected increase in

Table 1. Selected Bond Distances and Angles of Relevance for L/Cu^{II}-Br Deactivator Species^a

	$[Cu^{II}(TPMA)Br][Br]^{b}$	$[Cu^{II}(TPMA*^3)Br][Br]^c$	$[\mathrm{Cu^{II}}(\mathrm{TPMA^{NMe2}})\mathrm{Br}][\mathrm{Br}]^d$
Cu-N1 _{ax}	2.040(3)	2.028(3)	2.047(3)
Cu-N2 _{eq}	2.073(15)	2.059(3)	2.051(2)
Cu-N3 _{eq}	2.073(15)	2.149(3)	2.108(3)
Cu-N4 _{eq}	2.073(15)	2.044(3)	2.046(3)
Cu-Br ₁	2.384(6)	2.3740(5)	2.3898(6)
N_1 - Cu - N_2	80.86(5)	81.07(12)	80.59(10)
N_1 -Cu- N_3	80.86(5)	82.81(12)	80.60(10)
N_1 -Cu- N_4	80.86(5)	79.82(11)	81.42(10)
N_2 -Cu- N_3	117.53(3)	132.39(12)	126.78(10)
N_2 -Cu- N_4	117.53(3)	115.63(12)	116.34(10)
N_3 -Cu- N_4	117.53(3)	104.99(12)	109.40(10)
N_1 -Cu-Br ₁	180.00(5)	178.33(9)	179.89(9)
N_2 -Cu-Br ₁	99.14(5)	100.99(8)	98.59(8)
N_3 -Cu-Br ₁	99.14(5)	98.35(8)	99.49(7)
N_4 -Cu-Br $_1$	99.14(5)	97.27(8)	99.32(7)
$ au^e$	1.0	0.77	0.89

^aBond lengths are given in Angstroms and angles in degrees. ^bFrom ref 51. ^cFrom ref 42. ^dThis work. ^e τ parameter is calculated as $\tau = (\varphi_1 - \varphi_2)/60$, where φ_1 and φ_2 are the largest $(N_1-Cu-Br_1)$ and second largest (N_2-Cu-N_3) bond angles, $\tau=1$ (trigonal bipyramidal geometry), and $\tau=0$ (square pyramidal geometry).

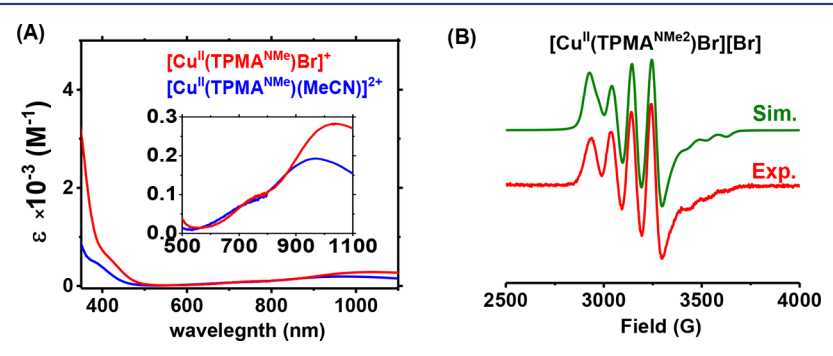


Figure 3. (A) Absorption spectra of the $[Cu^{II}(TPMA^{NMe2})Br]^+$ deactivator complex (red) and $[Cu^{II}(TPMA^{NMe2})(MeCN)]^{2+}$ complex (blue) in MeCN. $[CuX_2]_0 = 1$ mM (X = Br $^-$ or OTf $^-$). (B) Experimental (red) and simulated (green) X-band EPR spectra of the $[Cu^{II}(TPMA^{NMe2})Br][Br]$ complex in a 1:1 mixture of DCM:toluene recorded at 120 K ($g_1 = 2.173$, $A_1 = 255.3$ MHz, $g_2 = 2.198$, $A_2 = 336.5$ MHz, $g_3 = 1.95$, $A_3 = 260.1$ MHz).

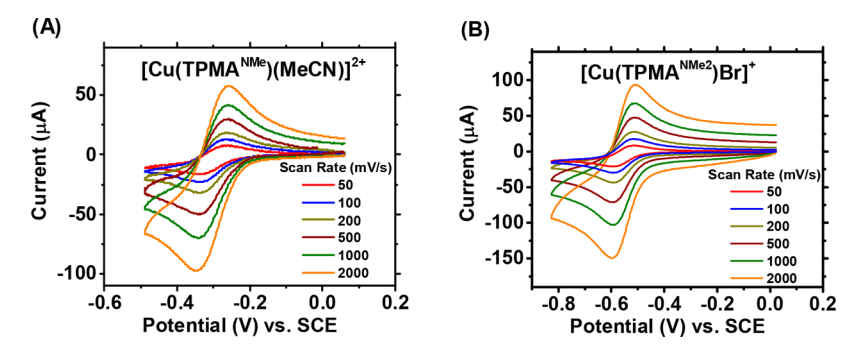


Figure 4. Cyclic voltammograms of (A) 1 mM $[Cu(TPMA^{NMe2})(MeCN)]^{2+}$ and (B) 1 mM $[Cu(TPMA^{NMe2})Br]^{+} + 20$ mM Et_4NBr in dry MeCN at different scan rates using Et_4NBF_4 as a supporting electrolyte and glassy carbon working electrode; $[L/Cu^{II}]_0 = 1$ mM.

current; peak separation also increases, revealing a quasireversible nature of the electron transfer. This shows that the TPMA^{NMe2} ligand is able to sufficiently stabilize the electrochemically generated Cu^I and indicates that these complexes have small rearrangement energies between the Cu^{I/II} oxidation states. Using eq 1, the β^{II}/β^{I} ratio was calculated as 1.1×10^{23} (Table 2), which is 1500 times larger than the previously reported value for the tris(2-dimethylaminoethyl)amine (Me₆TREN) complex in MeCN.⁵⁸ This large increase may be due to either a more stabilized Cu^{II} or a destabilized Cu^I. However, it was previously shown 43 that stability constants for $\mathrm{Cu^I}$ were similar using variously substituted pyridine-based ligands in DMF. 30

Upon introduction of coordinating bromide anions, the complex $[Cu(TPMA^{NMe2})Br]^+$ is formed and the redox potential shifts by -252 mV to give $E_{1/2}=-554$ mV vs SCE. K_{ATRP} increases roughly 1 order of magnitude for every 59 mV shift of redox potential, 26 indicating K_{ATRP} should be approximately 140 000 times greater relative to the unsubstituted TPMA-based catalyst, which has $E_{1/2}=-240$ mV vs

Table 2. Thermodynamic Properties of the $[Cu(L)(MeCN)]^{2+}$ and $[Cu(L)Br]^{+}$ Complexes in MeCN (L = TPMA, TPMA*³, TPMA^{NMe2})^a

	TPMA	TPMA*3	TPMA ^{NMe2}
E _{1/2,Cu} b	1.06	1.06	1.06
$E_{1/2,\mathrm{LCu}}$	-0.030^{d}	-0.177 ^c	-0.302
$E_{1/2, \text{LCuBr}}$	-0.240	-0.420	-0.554
$E_{1/2,Cu} - E_{1/2,LCu}$	1.090	1.237	1.362
$E_{1/2,\text{LCu}} - E_{1/2,\text{LCuBr}}$	0.210	0.243	0.252
$K_{\mathrm{Disp,Cu}}^{}e}$	1.0×10^{-21}	1.0×10^{-21}	1.0×10^{-21}
$K_{ m Disp,LCu}^{f}$	$<1.0 \times 10^{-4}$	$<1.0 \times 10^{-4}$	$<1.0 \times 10^{-4}$
$eta^{ m II}/eta^{ m I}$	2.7×10^{18}	8.1×10^{20}	1.1×10^{23}
$eta^{ ext{II}}/(eta^{ ext{I}})^2$	$< 1.0 \times 10^{17}$	$<1.0 \times 10^{17}$	$<1.0 \times 10^{17}$
$oldsymbol{eta}^{ ext{II}}$	$>7.1 \times 10^{19}$	$>6.6 \times 10^{24}$	$>1.1 \times 10^{29}$
$oldsymbol{eta}^{ ext{I}}$	$>2.7 \times 10^{1}$	$> 8.1 \times 10^3$	$>1.1 \times 10^6$
$eta_{ ext{X,app}}^{ ext{II}}/eta_{ ext{X,app}}^{ ext{I}}$	3.5×10^{3}	1.3×10^4	1.8×10^{3}
K_{ATRP}^{g}	$\sim 10^{-5}$	$\sim 10^{-3}$	$\sim 10^{-1}$
$k_{\rm a}~({\rm MBrP})$	$2.2 \times 10^{2} {}^{h}$	$8.4 \times 10^{3} i$	1.1×10^{6}

"Redox potentials in V vs SCE; $k_{\rm a}$ in M⁻¹ s⁻¹. ^bTaken from ref 62. ^cTaken from ref 43. ^dTaken from ref 46 using the conversion factor $E^{\rm o}({\rm Fc^+/Fc})=0.390~{\rm V}$ vs SCE. ^eFrom ref 61. ^fExperimental limiting value of $K_{\rm Disp,LCu}$. ^gEstimated for acrylates based on value of $E_{\rm 1/2,LCuBr}$ and the trend of $E_{\rm 1/2}$ vs $K_{\rm ATRP}$. ⁴³ ^hFrom ref 63. ⁱFrom ref 31.

SCE, ⁴⁶ and >10⁹ times greater than the original bpy catalyst, which has $E_{1/2}$ = +30 mV vs SCE. ⁶⁰ Furthermore, using eq 2, the $\beta_{\rm X,app}^{\rm II}/\beta_{\rm X,app}^{\rm I}$ ratio was calculated to be 1.8 × 10⁴, similar to that of other TPMA-based ligands in MeCN. ⁴³

$$K_{\text{disp,LCu}} = \frac{\left[LCu^{II}\right]_{eq} \left[L\right]_{eq}}{\left[LCu^{I}\right]_{eq}^{2}}$$
(3)

$$\frac{\beta^{\rm II}}{(\beta^{\rm I})^2} = \frac{K_{\rm disp,LCu}}{K_{\rm disp,Cu}} \tag{4}$$

Since cyclic voltammetry can only provide the β^{II}/β^I ratio, further analysis was carried out to estimate the individual β values. We previously reported⁴³ on the disproportionation equilibrium allowing for the calculation of $\beta^{II}/(\beta^I)^2$, as shown in eqs 3 and 4, where $K_{\rm disp,LCu}$ and $K_{\rm disp,Cu}$ are the equilibrium constants of disproportionation for ligated and solvated copper, respectively.⁴³ The determination of the disproportionation equilibrium, when coupled with electrochemical measurements, allows for the calculation of individual stability constants.

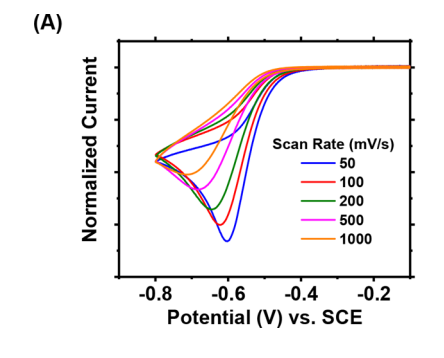
Analysis of $K_{\text{disp,LCu}}$ is difficult in MeCN due to the highly comproportionating nature of this solvent, i.e., very small values

of $K_{\rm disp}$. In fact, values of $K_{\rm disp,Cu}$ for the solvated ${\rm Cu}^{\rm I}$ complex in acetonitrile have previously been estimated on the order of $10^{-21.61}$ Therefore, it was only possible to estimate a limit of $K_{\rm disp,LCu} < 1.0 \times 10^{-4}$. Nonetheless, using this value the lower limits of $\beta^{\rm II}$ and $\beta^{\rm I}$ as 3.5×10^{29} and 1.9×10^{6} were estimated, respectively. These values, although likely underestimated due to uncertainty of $K_{\rm disp,LCu}$ are in good agreement with previously reported values for other ATRP catalysts. All thermodynamic parameters obtained in this study, as well as for TPMA and TPMA*3-based complexes, are summarized in Table 2. It should be noted that values of $\beta^{\rm I}$ are significantly limited by unattainable values of $K_{\rm disp,LCu}$ in MeCN.

Assessment of ATRP Activity. The ability of L/Cu^I complexes to activate (macro)alkyl halide bonds is paramount to the success of an ATRP system. The bond dissociation free energy (BDFE) of a C–X bond (X = Cl or Br) has been correlated to values of K_{ATRP} via DFT. Generally, the activation reaction is faster (larger values of k_a) if the resulting radical is more stabilized through either steric or resonance effects.

Electrochemistry is a useful tool in determining kinetic parameters in ATRP. The use of a rotating disk electrode allowed for measurement of $k_{\rm a}$ and $K_{\rm ATRP}$ for systems with moderately high activity ($k_{\rm a} < 10^4$). For more active processes such as in aqueous media and systems involving highly active catalysts, cyclic voltammetry of copper complexes under catalytic conditions (in the presence of RX) can be used to obtain $k_{\rm a}$. So be used to obtain $k_{\rm a}$. So be used from the current enhancement or degree of catalysis defined as $I_{\rm p}/I_{\rm p,0}$, where $I_{\rm p}$ and $I_{\rm p,0}$ stand for the cathodic peak current of the catalyst measured in the presence and absence of initiator, respectively (Figure SB). The procedure is described in the Supporting Information.

As shown in Figure 5A, cyclic voltammetry of the $[\mathrm{Cu}(\mathrm{TPMA}^{\mathrm{NMe2}})\mathrm{Br}]^+$ complex was conducted in the presence of methyl 2-bromopropionate (MBrP) and TEMPO. Here, MBrP acted as a small molecule model of acrylate chain end, while TEMPO was used as a radical trap to prevent the deactivation reaction. The dramatic increase in $I_p/I_{p,0}$, as the scan rate decreased, is consistent with previous reports. The absence of an oxidation peak indicates that the electrochemically generated Cu^{I} was completely consumed in the activation of MBrP, showing the high activity of this catalyst in the activation of acrylates. As shown in Figure S7, cyclic voltammetry under catalytic conditions gave a rate coefficient of activation, $k_{\mathrm{a}^{\prime}}$ of $(1.1 \pm 0.4) \times 10^6 \ \mathrm{M}^{-1} \ \mathrm{s}^{-1}$, which is the largest value reported for this initiator with copper-based ATRP catalysts. As will be shown later, values of k_{d} were calculated to



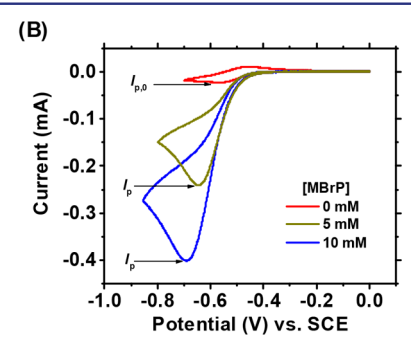
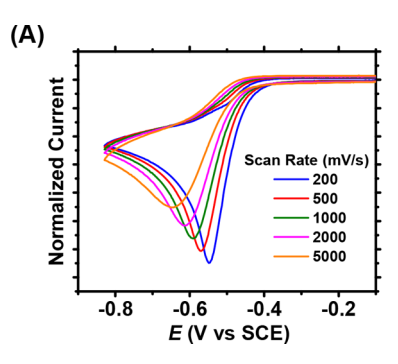


Figure 5. Cyclic voltammograms of $[Cu(TPMA^{NMe2})Br]^+$ in the presence of methyl 2-bromopropionate (MBrP; acrylate mimic) at (A) varying scan rates and (B) different $[MBrP]_0$ in MeCN at scan rate 0.2 V s⁻¹ at room temperature. In A current was normalized by dividing by square root of the scan rate. $[MBrP]_0$: $[TPMA^{NMe2}]_0$: $[CuBr_2]_0$: $[TEMPO]_0 = 0$ —10:1:1:10; $[CuBr_2]_0 = 1$ mM.

Journal of the American Chemical Society



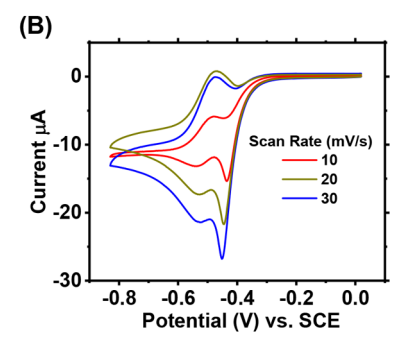
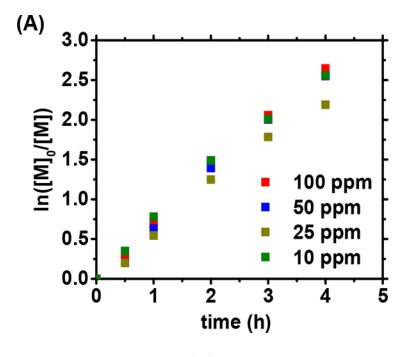


Figure 6. Cyclic voltammograms of 1 mM [Cu(TPMA^{NMe2})Br]⁺ in the presence of ethyl α-bromoisobutyrate (EBiB; methacrylate mimic) at (A) 5 and (B) 1 mM concentration in MeCN at room temperature. In A current was normalized by dividing by square root of the scan rate. [EBiB]₀: $[TPMA^{NMe2}]_0:[CuBr_2]_0:[TEMPO]_0 = 1-5:1:1:10.$



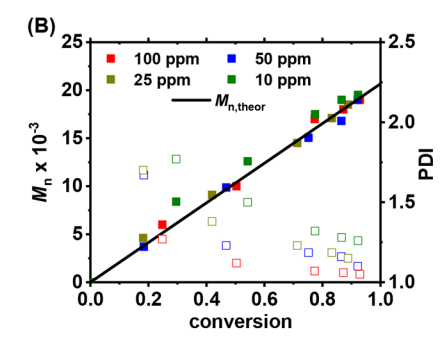


Figure 7. (A) Semilogarithmic plots and (B) M_n and D vs conversion for the ICAR ATRP of n-butyl acrylate (BA) at different $[Cu^{II}(TPMA^{NMe2})Br][Br]$ loadings under the initial conditions $[BA]_0$: $[EBiB]_0$: $[L/CuBr_2]_0$: $[TPMA^{NMe2}]_0$: $[AIBN]_0 = 160$:1:0.016-0.0016:0.2 in anisole at 60 °C; catalyst loadings in ppm vs monomer; [BA]₀ = 4.5 M.

be 5 \times 10⁷ M⁻¹ s⁻¹. Thus, $K_{\rm ATRP}$ was estimated to be on the order of 10⁻¹. This value is consistent with that estimated from the redox potential (Table 2, $K_{ATRP} = 1.0 \times 10^{-1}$). This also indicated that deactivation for so active and reducing complexes is still very efficient. These preliminary studies further indicate that this new complex is the most active copper-based ATRP catalyst to date.

Figure 6A shows the cyclic voltammetry of [Cu(TPMA^{NMe2})-Br] in the presence of more active ethyl α -bromoisobutyrate (EBiB; methacrylate mimic). With $[EBiB]_0 \gg$ [Cu^{II}(TPMA^{NMe2})Br]₀ a large increase of the cathodic current and complete disappearance of the anodic peak was observed, similar to the voltammograms in the presence of the less active MBrP. Cyclic voltammetry under catalytic conditions gave k_a = $(7.2 \pm 2.0) \times 10^6 \text{ M}^{-1} \text{ s}^{-1}$, indicating that K_{ATRP} approaches unity. However, at a ratio of $[Cu^{II}(TPMA^{NMe2})Br]_0$: $[EBiB]_0 =$ 1, an interesting cyclic voltammogram was observed where the cathodic wave splits into two peaks (Figure 6B). This particular phenomenon is attributed to "total catalysis", which is usually found for extremely efficient catalysts with rate constants for bimolecular reactions $>10^6 \,\mathrm{M}^{-1} \,\mathrm{s}^{-1}.^{69}$ Indeed, in this case, only an infinitesimal amount of L/Cu^I is required for the complete reduction of RBr, giving a first irreversible peak at $E > E_{1/2,LCuBr}$ due to the very fast catalytic reduction of EBiB. On the other hand, the electrochemical reduction of $[Cu(TPMA^{NMe2})Br]^+$ is still reversible since the majority of the catalyst is not involved in the electrocatalytic process. Overall, these results show the extreme reactivity of [Cu(TPMANMe2)Br]+, which can be used in ATRP with unprecedentedly low parts per million

Low Parts Per Million ATRP of Acrylates. To assess the efficiency of the [Cu(TPMANMe2)Br]+ catalyst, various forms of ATRP with activator regeneration were conducted. First, ICAR ATRP was conducted at catalyst loadings ranging from 10 to 100 ppm relative to monomer with 2,2'-azobis(2-isobutyronitrile) (AIBN) as radical initiator. 70 As shown in Figure 7, linear semilogarithmic plots vs time were observed at all catalyst loadings. This is consistent with previously established ICAR kinetics with bimolecular termination for which the amount of catalyst does not change the rate of polymerization as shown in eq 5, where f is initiator efficiency of AIBN, k_{azo} is the decomposition rate coefficient, and k_t is the rate coefficient of radical-radical termination.^{71,72}

$$[R^{\bullet}] = \sqrt{\frac{fk_{\text{azo}}[\text{AIBN}]}{k_{\text{t}}}}$$
 (5)

$$[\mathbf{R}^{\bullet}] = \frac{fk_{\text{azo}}[\text{AIBN}]}{k_{\text{CRT}}^{\text{app}}[\text{Cu}^{\text{I}}]}$$
(6)

After 4 h, >90% conversion was achieved for all reactions with a linear increase of molecular weights with conversion, typical of a well-controlled polymerization. While the rate of polymerization was unaffected by the initial amount of catalyst, molecular weight distributions gradually broadened upon decreasing catalyst concentration (Figure S9). This is attributed to decreased rate of deactivation relative to propagation. Although the initial amount of catalyst does not affect the rate of polymerization, at lower catalyst loadings there is less deactivator complex to reversibly trap radicals. This causes more monomer additions per activation cycle and thus a broadening of the molecular weight distribution. (cf. eq 7)

An interesting point to note is that according to the kinetic plots presented in Figure 7A and PREDICI simulations provided in the SI, bimolecular radical termination (RT) should dominate catalytic radical termination (CRT), contrary to previous studies with other ATRP catalysts. ¹³ If CRT would significantly contribute to overall termination, the polymerization kinetics would depend on catalyst concentration (eq 6), where $k_{\rm CRT}^{\rm app}$ is the apparent CRT rate coefficient. ⁷³ This is because, as shown in Scheme 3, CRT requires the coordination of a propagating radical ($P_{\rm n}^{\bullet}$) to the L/Cu^I complex to form a L/Cu^{II}- $P_{\rm n}$ organometallic species. ⁷³

Scheme 3. Interplay between Conventional Bimolecular Radical Termination (RT) and Catalytic Radical Termination via the Reactive $L/Cu^{II}-P_n$ Intermediate in ATRP of Acrylates

$$L/Cu^{l} + P_{n}^{\bullet} \xrightarrow{k_{add}} L/Cu^{l} - P_{n} \xrightarrow{k_{CRT}[P_{m}^{\bullet}]} L/Cu^{l} + P_{n} + P_{m}$$

$$P_{m}^{\bullet} \xrightarrow{k_{t}} P_{n} - P_{m}$$

Since the L/Cu^I concentration in ICAR ATRP is governed by the dynamic ATRP equilibrium⁷⁴ (Scheme 1) and considering the very high values of $K_{\rm ATRP} \approx 10^{-1}$ for this system, the amount of TPMA^{NMe2}/Cu^I present in solution is calculated to be 9.6×10^{-10} at equilibrium (see Supporting Information for calculation).⁷⁴ In other words, a radical will kinetically terminate with a second radical faster than it will coordinate to trace amounts of TPMA^{NMe2}/Cu^I. This should still happen, even if addition of a radical to TPMA^{NMe2}/Cu^I occurs at diffusion-controlled rates ($k_{\rm add} = 10^8 \, {\rm M}^{-1} \, {\rm s}^{-1}$). This is not the case of less active catalysts such as TPMA-based systems ($K_{\rm ATRP} \approx 10^{-5}$),⁶³ where CRT dominates because of a relatively higher concentration of TPMA/Cu^I of $1.8 \times 10^{-6} \, {\rm M}$. As shown in Figure S10, these findings are supported by PREDICI simulations: the much more active TPMA^{NMe2}-based system kinetically suppressed CRT because only a small

fraction of $TPMA^{NMe2}/Cu^I$ is present in solution, resulting in a relatively larger fraction of living chains compared to less active systems.

Then Ag⁰ ATRP, a form of ARGET ATRP, was conducted to further test the scope of the newly synthesized catalyst. Ag⁰ ATRP employs silver wire to heterogeneously reduce L/Cu^{II} to L/Cu^I with oxidation of Ag⁰ to Ag^IBr. 11 As shown in Figure 8, the TPMA^{NMe2} catalyst successfully polymerized MA via Ag⁰ ARGET ATRP using as little as 10 ppm of catalyst relative to monomer. However, at 5 ppm, the polymerization was no longer living as confirmed by the molecular weights decreasing with conversion and high D values (>1.5). Since the rate of Ag ARGET ATRP depends on the rate of Cu^I generation, the linear semilogarithmic kinetic plots showed that Cu^{II} was still reduced but unable to efficiently deactivate radicals. This is because at such low catalyst concentrations the rates of propagation and termination are competing with the rate of deactivation. Thus, it is likely that 10 ppm is around the lowest possible limits to achieve a well-controlled polymerization in copper-catalyzed ATRP of acrylates. Nevertheless, unprecedented control was achieved using as little as 10 ppm of catalyst for the polymerization of acrylates. The nearly colorless nature of the polymerization solution at 10 ppm can be seen in Figure

Using the results from the two polymerization systems shown in Figures 6 and 7, one can estimate the rate coefficient of deactivation, $k_{\rm d}$, according to eq 7, where DP is the degree of polymerization, $k_{\rm p}$ is the propagation rate constant, and p is monomer conversion.

$$M_{\rm w}/M_{\rm n} = 1 + \frac{1}{\rm DP} + \left(\frac{k_{\rm p}[{\rm RX}]}{k_{\rm d}[{\rm LCu^{II}} - {\rm X}]}\right) \left(\frac{2}{p} - 1\right)$$
 (7)

Due to the negligible amount of termination, it has been assumed that $[RX] = [RX]_0$. Furthermore, since the K_{ATRP} is so large, it can be assumed that essentially all copper is in the form of $L/Cu^{II}-X$ and therefore $[L/Cu^{II}-X] = [L/Cu^{II}-X]_0$. Using

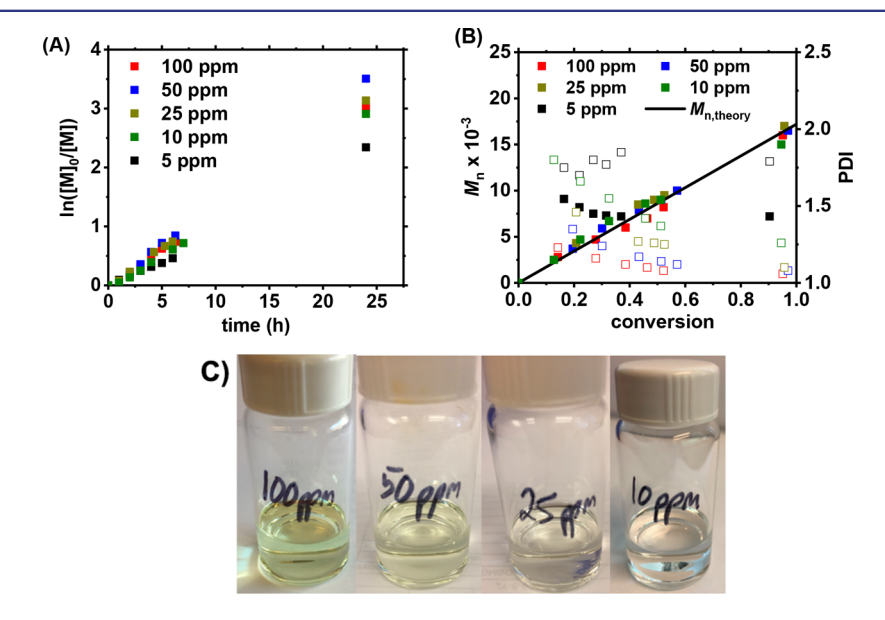


Figure 8. (A) Semilogarithmic plots and (B) M_n and D vs conversion for the Ag^0 ATRP of methyl acrylate (MA) at different loadings of $[Cu^{II}(TPMA^{NMe2})Br][Br]$ under the initial conditions $[MA]_0$: $[EBiB]_0$: $[Cu^{II}(TPMA^{NMe2})Br][Br]_0$ = 200:1:0.02–0.002 with 10 cm Ag^0 wire (SA/V) = 0.53 cm⁻¹ in DMF at 50 °C; catalyst loadings in ppm vs monomer; $[MA]_0$ = 5.75 M. (C) Pictures of polymerization solution at decreasing catalyst loadings of $[Cu^{II}(TPMA^{NMe2})Br][Br]$.

the final dispersity data of the polymerizations in Figures 7 and $8, k_d = (5.4 \pm 1.7) \times 10^7 \,\mathrm{M}^{-1} \,\mathrm{s}^{-1}$ was obtained which gives an estimated value of $K_{ATRP} = 2.2 \times 10^{-2}$ for acrylate systems. This indicates that the degree of substitution and redox potential of pyridinic-based catalysts have very little effect on k_d . Instead, only the total amount of Cu^{II}-X deactivator, which is regulated by $[Cu^{II}]_0$ and K_{ATRP} , will define the level of control in a particular ATRP system with activator regeneration.

Comparison of TPMA^{NMe2} to Other Ligands in ATRP.

As shown in Figure 9, the redox potential scales linearly with

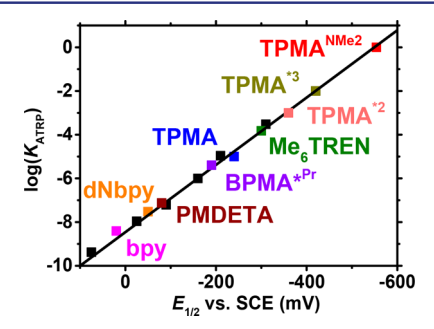


Figure 9. Redox potential $(E_{1/2})$ vs $\log(K_{ATRP})$ for various ATRP catalysts complexed by multidentate nitrogen-based ligands. Values for $E_{1/2}$ have previously been determined experimentally vs an SCE electrode in MeCN at room temperature. Values of $K_{\rm ATRP}$ are for ethyl α-bromoisobutyrate (EBiB; methacrylate mimic) in MeCN at room temperature. Structures of all ligands are shown in Figure S11.

 $log(K_{ATRP})$ for EBiB in MeCN at room temperature for a variety of ligands (Figure S11 for structures of ligands). On the basis of $E_{1/2}$ values, the newly synthesized TPMA^{NMe2}-based catalyst ($E_{1/2} = -554$ mV) is almost 10 billion times more active than seminal bpy-based catalyst ($E_{1/2}$ = +30 mV). Even looking at catalysts which are widely used for low parts per million ATRP, the TPMANMe2-based system is ~300 000 and 30 000 times more active than the TPMA- $(E_{1/2} = -240 \text{ mV})$ and Me₆TREN ($E_{1/2} = -300 \text{ mV}$)-based catalysts, respectively. Unfortunately, with such a highly active catalyst as [Cu-(TPMANMe2)]+, activation of alkyl halides approaches diffusioncontrolled limits ($k_a > 10^6 \text{ M}^{-1} \text{ s}^{-1}$), and with already diffusioncontrolled deactivation rates ($k_d = > 10^7 \text{ M}^{-1} \text{ s}^{-1}$), values of K_{ATRP} begin to approach unity. This would mean that for commonly used monomers such as acrylates and methacrylates, this catalytic system may be the upper limit of activity since the only way to further increase K_{ATRP} would be to decrease k_d . This is not best since the control achieved in ATRP is due to fast rates of deactivation. Encouragingly, the high ATRP activity provided by the TPMANMe2-based catalyst can open the possibility to polymerize less active monomers such as vinyl acetate and N-vinylpyrrolidone which have historically fallen victim to too low values of K_{ATRP} .

CONCLUSIONS

The synthesis of a new ATRP catalyst employing the pdimethylamino-substituted TPMA ligand, tris[(4dimethylaminiopyridyl)methyl]amine (TPMANMe2), is reported. Variable-temperature NMR showed a fluxional Cu^I complex with rapid ligand exchange. In the solid state, the $\left[Cu^{II}(TPMA^{NMe^2})Br\right]^+$ complex exhibited nearly perfect trigonal bipyramidal geometry. UV-vis and EPR confirmed that this geometry was retained in solution. Electrochemical measurements showed a quasi-reversible $\text{TPMA}^{\text{NMe2}}\text{Cu}^{\text{I/II}}$

couple, indicating small geometric rearrangement throughout the redox cycle. Stability constants for Cu^{II} and Cu^{III} were comparable to other copper ATRP catalysts in MeCN. Electrochemistry was also utilized to assess the activation of methyl 2-bromopropionate (MBrP; acrylate mimic) and ethyl α -bromoisobutyrate, for which a rate coefficient of activation was measured as $k_a = 1.1 \times 10^6$ and 7.2×10^6 M⁻¹ s⁻¹, respectively. This leads to an estimation of $K_{\rm ATRP} = 2.2 \times 10^{-2}$ and 7.2×10^{-1} , respectively, which indicated this is the most active ATRP catalyst to date. A large value of $k_d > 10^7 \text{ M}^{-1} \text{ s}^{-1}$ was calculated and indicated that the catalyst is also a good deactivator. Both ICAR and Ag⁰ ATRP of acrylates were well controlled using as little as 10 ppm of catalyst relative to monomer. Encouragingly, due to the high values of K_{ATRP} and low [TPMA^{NMe2}/Cu^I], unwanted side reactions involving Cu^I such as catalytic radical termination (CRT) are suppressed leading to higher chain-end functionality. Furthermore, this catalyst can potentially allow for the successful ATRP of less active monomers. Investigations in this direction are currently ongoing in our laboratories.

ASSOCIATED CONTENT

Supporting Information

The Supporting Information is available free of charge on the ACS Publications website at DOI: 10.1021/jacs.7b12180.

Crystal structure details for $C_{24}H_{35.50}Br_2CuN_7O_{1.50}$ (CIF) Experimental procedures, X-ray diffraction details, discussion of electrochemical methods, GPC traces, example calculations of L/Cu^I at steady state, kinetic simulations, and structures of common ligands employed in ATRP (PDF)

AUTHOR INFORMATION

Corresponding Author

*km3b@andrew.cmu.edu

ORCID

Rinaldo Poli: 0000-0002-5220-2515

Krzysztof Matyjaszewski: 0000-0003-1960-3402

Author Contributions

[‡]T.R. and M.F. contributed equally.

The authors declare no competing financial interest.

ACKNOWLEDGMENTS

Support from the NSF (CHE 1707490) is acknowledged. We thank the Centre National de la Recherche Scientifique (CNRS) for support through the PICS06782 grant and through the Laboratoire International Associé (LIA) "Laboratory of Coordination Chemistry for Controlled Radical Polymerization". We are also grateful to the French Embassy in Washington D.C. for a Chateaubriand Fellowship to T.R. We acknowledge Mateusz Olszewski for designing the graphical abstract for this manuscript.

REFERENCES

- (1) Matyjaszewski, K.; Xia, J. Chem. Rev. 2001, 101 (9), 2921–2990.
- (2) Wang, J.-S.; Matyjaszewski, K. J. Am. Chem. Soc. 1995, 117 (20),
- (3) Kato, M.; Kamigaito, M.; Sawamoto, M.; Higashimura, T. Macromolecules 1995, 28 (5), 1721-1723.
- (4) Matyjaszewski, K. Macromolecules 2012, 45 (10), 4015-4039.

- (5) Wang, J.-S.; Matyjaszewski, K. Macromolecules 1995, 28 (23), 7901-7910.
- (6) Matyjaszewski, K.; Tsarevsky, N. V. J. Am. Chem. Soc. 2014, 136 (18), 6513-6533.
- (7) Matyjaszewski, K.; Jakubowski, W.; Min, K.; Tang, W.; Huang, J.; Braunecker, W. A.; Tsarevsky, N. V. *Proc. Natl. Acad. Sci. U. S. A.* **2006**, 103 (42), 15309–15314.
- (8) Konkolewicz, D.; Magenau, A. J. D.; Averick, S. E.; Simakova, A.; He, H.; Matyjaszewski, K. *Macromolecules* **2012**, *45* (11), 4461–4468.
- (9) Chan, N.; Cunningham, M. F.; Hutchinson, R. A. Macromol. Chem. Phys. 2008, 209 (17), 1797–1805.
- (10) Jakubowski, W.; Matyjaszewski, K. Angew. Chem. 2006, 118 (27), 4594–4598.
- (11) Williams, V. A.; Ribelli, T. G.; Chmielarz, P.; Park, S.; Matyjaszewski, K. J. Am. Chem. Soc. **2015**, 137 (4), 1428–1431.
- (12) Konkolewicz, D.; Wang, Y.; Zhong, M.; Krys, P.; Isse, A. A.; Gennaro, A.; Matyjaszewski, K. *Macromolecules* **2013**, *46* (22), 8749–8772.
- (13) Ribelli, T. G.; Konkolewicz, D.; Bernhard, S.; Matyjaszewski, K. J. Am. Chem. Soc. **2014**, 136 (38), 13303–13312.
- (14) Pan, X.; Tasdelen, M. A.; Laun, J.; Junkers, T.; Yagci, Y.; Matyjaszewski, K. Prog. Polym. Sci. 2016, 62, 73–125.
- (15) Anastasaki, A.; Nikolaou, V.; Zhang, Q.; Burns, J.; Samanta, S. R.; Waldron, C.; Haddleton, A. J.; McHale, R.; Fox, D.; Percec, V.; Wilson, P.; Haddleton, D. M. J. Am. Chem. Soc. 2014, 136 (3), 1141–1149.
- (16) Discekici, E. H.; Anastasaki, A.; Kaminker, R.; Willenbacher, J.; Truong, N. P.; Fleischmann, C.; Oschmann, B.; Lunn, D. J.; Read de Alaniz, J.; Davis, T. P.; Bates, C. M.; Hawker, C. J. *J. Am. Chem. Soc.* **2017**, *139* (16), 5939–5945.
- (17) Anastasaki, A.; Oschmann, B.; Willenbacher, J.; Melker, A.; Van Son, M. H. C.; Truong, N. P.; Schulze, M. W.; Discekici, E. H.; McGrath, A. J.; Davis, T. P.; Bates, C. M.; Hawker, C. J. Angew. Chem., Int. Ed. 2017, 56 (46), 14483–14487.
- (18) Chmielarz, P.; Fantin, M.; Park, S.; Isse, A. A.; Gennaro, A.; Magenau, A. J. D.; Sobkowiak, A.; Matyjaszewski, K. *Prog. Polym. Sci.* **2017**, *69*, 47–78.
- (19) Wang, Z.; Pan, X.; Li, L.; Fantin, M.; Yan, J.; Wang, Z.; Wang, Z.; Xia, H.; Matyjaszewski, K. *Macromolecules* **2017**, *50* (20), 7940–7948
- (20) Mohapatra, H.; Kleiman, M.; Esser-Kahn, A. P. Nat. Chem. **2017**, 9 (2), 135–139.
- (21) Lin, C. Y.; Coote, M. L.; Gennaro, A.; Matyjaszewski, K. J. Am. Chem. Soc. 2008, 130 (38), 12762–12774.
- (22) Coessens, V.; Pintauer, T.; Matyjaszewski, K. Prog. Polym. Sci. **2001**, 26 (3), 337–377.
- (23) Tang, W.; Tsarevsky, N. V.; Matyjaszewski, K. J. Am. Chem. Soc. **2006**, 128 (5), 1598–1604.
- (24) Tsarevsky, N. V.; Braunecker, W. A.; Tang, W.; Matyjaszewski, K. ACS Symp. Ser. 2009, 1023, 85–96.
- (25) Braunecker, W. A.; Tsarevsky, N. V.; Gennaro, A.; Matyjaszewski, K. Macromolecules 2009, 42 (17), 6348-6360.
- (26) Tang, W.; Kwak, Y.; Braunecker, W.; Tsarevsky, N. V.; Coote, M. L.; Matyjaszewski, K. J. Am. Chem. Soc. 2008, 130 (32), 10702–10713.
- (27) Gillies, M. B.; Matyjaszewski, K.; Norrby, P.-O.; Pintauer, T.; Poli, R.; Richard, P. *Macromolecules* **2003**, *36* (22), 8551–8559.
- (28) Tang, W.; Matyjaszewski, K. Macromolecules 2006, 39 (15), 4953-4959.
- (29) Tsarevsky, N. V.; Braunecker, W. A.; Vacca, A.; Gans, P.; Matyjaszewski, K. *Macromol. Symp.* **2007**, 248 (1), 60–70.
- (30) Rorabacher, D. B. Chem. Rev. 2004, 104 (2), 651-698.
- (31) Schroder, K.; Mathers, R. T.; Buback, J.; Konkolewicz, D.; Magenau, A. J. D.; Matyjaszewski, K. ACS Macro Lett. 2012, 1 (8), 1037–1040.
- (32) Lee, J. Y.; Peterson, R. L.; Ohkubo, K.; Garcia-Bosch, I.; Himes, R. A.; Woertink, J.; Moore, C. D.; Solomon, E. I.; Fukuzumi, S.; Karlin, K. D. J. Am. Chem. Soc. **2014**, 136 (28), 9925–9937.

- (33) Magenau, A. J. D.; Kwak, Y.; Schröder, K.; Matyjaszewski, K. ACS Macro Lett. 2012, 1 (4), 508-512.
- (34) Zhang, C. X.; Kaderli, S.; Costas, M.; Kim, E.-i.; Neuhold, Y.-M.; Karlin, K. D.; Zuberbühler, A. D. *Inorg. Chem.* **2003**, *42* (6), 1807–1824
- (35) Comba, P.; Morgen, M.; Wadepohl, H. *Inorg. Chem.* **2013**, 52 (11), 6481–6501.
- (36) Kim, S.; Lee, J. Y.; Cowley, R. E.; Ginsbach, J. W.; Siegler, M. A.; Solomon, E. I.; Karlin, K. D. *J. Am. Chem. Soc.* **2015**, *137* (8), 2796–2799.
- (37) Solomon, E. I.; Sundaram, U. M.; Machonkin, T. E. Chem. Rev. **1996**, 96 (7), 2563–2606.
- (38) Solomon, E. I.; Heppner, D. E.; Johnston, E. M.; Ginsbach, J. W.; Cirera, J.; Qayyum, M.; Kieber-Emmons, M. T.; Kjaergaard, C. H.; Hadt, R. G.; Tian, L. *Chem. Rev.* **2014**, *114* (7), 3659–3853.
- (39) Wilmot, C. M.; Hajdu, J.; McPherson, M. J.; Knowles, P. F.; Phillips, S. E. V. Science 1999, 286 (5445), 1724–1728.
- (40) Solomon, E. I.; Chen, P.; Metz, M.; Lee, S.-K.; Palmer, A. E. Angew. Chem., Int. Ed. **2001**, 40 (24), 4570–4590.
- (41) Decker, H.; Dillinger, R.; Tuczek, F. Angew. Chem., Int. Ed. **2000**, 39 (9), 1591–1595.
- (42) Fry, H. C.; Lucas, H. R.; Narducci Sarjeant, A. A.; Karlin, K. D.; Meyer, G. J. *Inorg. Chem.* **2008**, *47* (1), 241–256.
- (43) Kaur, A.; Ribelli, T. G.; Schröder, K.; Matyjaszewski, K.; Pintauer, T. Inorg. Chem. 2015, 54 (4), 1474–1486.
- (44) Wang, Y.; Zhong, M.; Zhu, W.; Peng, C.-H.; Zhang, Y.; Konkolewicz, D.; Bortolamei, N.; Isse, A. A.; Gennaro, A.; Matyjaszewski, K. *Macromolecules* **2013**, *46* (10), 3793–3802.
- (45) Mason, J. Chem. Rev. 1987, 87 (6), 1299-1312.
- (46) Eckenhoff, W. T.; Garrity, S. T.; Pintauer, T. Eur. J. Inorg. Chem. **2008**, 2008 (4), 563-571.
- (47) Hsu, S. C. N.; Chien, S. S. C.; Chen, H. H. Z.; Chiang, M. Y. J. Chin. Chem. Soc. **2007**, 54 (3), 685–692.
- (48) Kitagawa, S.; Munakata, M. Inorg. Chem. 1981, 20 (7), 2261–2267.
- (49) Kitagawa, S.; Munakata, M.; Miyaji, N. Inorg. Chem. **1982**, 21 (10), 3842–3843.
- (50) Munakata, M.; Kitagawa, S.; Kosome, S.; Asahara, A. *Inorg. Chem.* **1986**, 25 (15), 2622–2627.
- (51) Thompson, J. S.; Swiatek, R. M. Inorg. Chem. 1985, 24 (1), 110-113.
- (52) Eckenhoff, W. T.; Pintauer, T. Inorg. Chem. 2010, 49 (22), 10617–10626.
- (53) Zerk, T. J.; Bernhardt, P. V. Coord. Chem. Rev. 2017, DOI: 10.1016/j.ccr.2017.11.016.
- (54) Hiskey, M. A.; Ruminski, R. R. Inorg. Chim. Acta 1986, 112 (2), 189-195.
- (55) McLachlan, G. A.; Fallon, G. D.; Martin, R. L.; Spiccia, L. *Inorg. Chem.* **1995**, 34 (1), 254–261.
- (56) Pintauer, T.; Qiu, J.; Kickelbick, G.; Matyjaszewski, K. Inorg. Chem. 2001, 40 (12), 2818–2824.
- (57) Zerk, T. J.; Bernhardt, P. V. Inorg. Chem. 2017, 56 (10), 5784-5792.
- (58) Bortolamei, N.; Isse, A. A.; Di Marco, V. B.; Gennaro, A.; Matyjaszewski, K. *Macromolecules* **2010**, 43 (22), 9257–9267.
- (59) De Paoli, P.; Isse, A. A.; Bortolamei, N.; Gennaro, A. Chem. Commun. 2011, 47 (12), 3580-3582.
- (60) Qiu, J.; Matyjaszewski, K.; Thouin, L.; Amatore, C. Macromol. Chem. Phys. **2000**, 201 (14), 1625–1631.
- (61) Ahrland, S.; Nilsson, K.; Tagesson, B.; Haaland, A.; Schilling, B. E. R.; Seip, R.; Taugbøl, K. Acta Chem. Scand. 1983, 37a, 193–201.
- (62) Gritzner, G. J. Phys. Chem. 1986, 90 (21), 5478-5485.
- (63) Ribelli, T. G.; Augustine, K. F.; Fantin, M.; Krys, P.; Poli, R.; Matyjaszewski, K. *Macromolecules* **2017**, *50* (20), 7920–7929.
- (64) Fantin, M.; Isse, A. A.; Matyjaszewski, K.; Gennaro, A. *Macromolecules* **2017**, *50* (7), 2696–2705.
- (65) Bell, C. A.; Bernhardt, P. V.; Monteiro, M. J. J. Am. Chem. Soc. **2011**, 133 (31), 11944–11947.

- (66) Fantin, M.; Lorandi, F.; Gennaro, A.; Isse, A.; Matyjaszewski, K. Synthesis **2017**, 49 (15), 3311–3322.
- (67) Bortolamei, N.; Isse, A. A.; Magenau, A. J. D.; Gennaro, A.; Matyjaszewski, K. *Angew. Chem., Int. Ed.* **2011**, 50 (48), 11391–11394.
- (68) Fantin, M.; Isse, A. A.; Gennaro, A.; Matyjaszewski, K. *Macromolecules* **2015**, 48 (19), 6862–6875.
- (69) Savéant, J. M.; Su, K. B. J. Electroanal. Chem. Interfacial Electrochem. 1984, 171 (1), 341–349.
- (70) D'Hooge, D. R.; Konkolewicz, D.; Reyniers, M.-F.; Marin, G. B.; Matyjaszewski, K. *Macromol. Theory Simul.* **2012**, *21* (1), 52–69.
- (71) Ribelli, T. G.; Konkolewicz, D.; Pan, X.; Matyjaszewski, K. *Macromolecules* **2014**, 47 (18), 6316–6321.
- (72) Krys, P.; Matyjaszewski, K. Eur. Polym. J. 2017, 89, 482-523.
- (73) Ribelli, T. G.; Wahidur Rahaman, S. M.; Daran, J.-C.; Krys, P.; Matyjaszewski, K.; Poli, R. *Macromolecules* **2016**, 49 (20), 7749–7757.
- (74) Krys, P.; Ribelli, T. G.; Matyjaszewski, K.; Gennaro, A. *Macromolecules* **2016**, 49 (7), 2467–2476.
- (75) Barner-Kowollik, C.; Beuermann, S.; Buback, M.; Castignolles, P.; Charleux, B.; Coote, M. L.; Hutchinson, R. A.; Junkers, T.; Lacik, I.; Russell, G. T.; Stach, M.; van Herk, A. M. *Polym. Chem.* **2014**, *5* (1), 204–212.